Journal of Respiration

MDPI

Article

Genotype–Computed Tomography Phenotype of the *RSPH4A* Founder Variant in Primary Ciliary Dyskinesia

Josué E. Pabón Maldonado [1,*], Gabriel Rosario-Ortiz [1], Marcos J. Ramos-Benitez [1], Ricardo A. Mosquera [2] and Wilfredo De Jesús-Rojas [1,*]

[1] Department of Pediatrics and Basic Science, Ponce Health Sciences University, Ponce, PR 00716, USA; grosario24@stu.psm.edu (G.R.-O.); mjramos@psm.edu (M.J.R.-B.)
[2] Department of Pediatrics, McGovern Medical School at UTHealth Houston, Houston, TX 77030, USA; ricardo.a.mosquera@uth.tmc.edu
* Correspondence: jpabon22@stu.psm.edu or jpabon22@psmhs.onmicrosoft.com (J.E.P.M.); wdejesus@psm.edu (W.D.J.-R.)

Abstract

Background/Objectives: Primary ciliary dyskinesia (PCD) caused by biallelic *RSPH4A* variants is enriched in the Puerto Rican population due to the founder allele c.921+3_921+6delAAGT, a 4-nucleotide deletion affecting the intron 6 splice donor. This study aimed to characterize the genotype–computed tomography (CT) phenotype associated with homozygosity for this founder variant and examine relationships among age, pulmonary function, and structural lung disease. Methods: We performed a cross-sectional analysis of 20 genetically confirmed patients homozygous for *RSPH4A* c.921+3_921+6delAAGT. Demographic characteristics, spirometry, and chest CT findings were evaluated. Structural disease burden was quantified using a Bhalla-style CT severity score, and regression analyses assessed associations among age, CT severity, sex, and forced expiratory volume in 1 s (FEV_1). Results: Mean FEV_1 was 48.9% predicted (range, 26–65%) and showed no measurable association with age (slope −0.02% per year; 95% CI, −0.26 to +0.22; $p = 0.88$). Bronchiectasis was multilobar, with right-middle-lobe involvement in 80% of patients. CT severity showed a modest cross-sectional increase with age, whereas FEV_1 remained relatively stable across age groups. In multivariable analysis, greater CT severity showed the strongest association with lower FEV_1 ($\beta = -0.56\%$ per CT point; 95% CI, −1.13 to +0.01; $p = 0.07$), although this association did not reach statistical significance. Conclusions: In this Puerto Rican *RSPH4A* founder cohort, substantial airflow obstruction was observed across the age spectrum, while structural CT abnormalities were greater in older patients despite relatively stable FEV_1. This cross-sectional dissociation suggests that spirometry alone may incompletely reflect structural disease burden. These findings support the complementary role of CT imaging in phenotypic characterization and longitudinal assessment of *RSPH4A*-related PCD and provide a rationale for earlier identification and future longitudinal studies.

Keywords: primary ciliary dyskinesia; *RSPH4A*; founder genetic variant; Puerto Rico; bronchiectasis; FEV_1; chest CT; genotype–phenotype

Check for updates

Academic Editors: Janice Wang and Patricia A. Walker

Received: 16 August 2026
Revised: 16 September 2026
Accepted: 28 September 2026
Published: 2 October 2026

Copyright: © 2026 by the authors. Licensee MDPI, Basel, Switzerland. This article is an open access article distributed under the terms and conditions of the Creative Commons Attribution (CC BY) license.

1. Introduction

Primary ciliary dyskinesia (PCD) is an autosomal-recessive ciliopathy characterized by impaired mucociliary clearance, neonatal respiratory distress, chronic rhinosinusitis, otitis media, and progressive bronchiectasis [1]. Its estimated prevalence is approximately

1:7500 [2], and more than 60 causative genes have been identified [1]. The *RSPH4A* gene encodes a structural component of the ciliary radial spoke head, an indispensable element of the central pair–radial spoke complex that coordinates ciliary beat [3,4]. Pathogenic *RSPH4A* variants typically produce a central-pair defect on transmission electron microscopy, a rotational ciliary beat pattern on high-speed video microscopy, and absent or markedly reduced nasal nitric oxide [5,6]. Within Puerto Rico, *RSPH4A*-related PCD is unusually common because of a founder variant, designated at the DNA level as *RSPH4A* c.921+3_921+6delAAGT, a 4-nucleotide deletion affecting the conserved +3 to +6 positions of the intron 6 splice donor site [7,8]. The variant is predicted to cause aberrant splicing-exon 6 skipping or intron retention, generating frameshift transcripts that are degraded by nonsense-mediated decay; functionally it behaves as a near-null (loss-of-function) allele [8]. Despite its importance on the island, the clinical, functional, and imaging consequences of the Puerto Rican *RSPH4A* founder variant have not been described in a unified cohort [9]. We therefore performed a genotype–phenotype analysis restricted to patients homozygous for c.921+3_921+6delAAGT. The aims were to: (1) describe demographics, spirometry, and chest CT severity; (2) estimate age-related patterns of lung function and structural disease; (3) assess sex-based differences; (4) identify multivariable predictors of FEV_1; and (5) place the findings in the context of allele biology and the Puerto Rican founder effect.

2. Materials and Methods

2.1. Cohort and Data Acquisition

The analysis included 20 patients (n = 20) with genetically confirmed *RSPH4A* PCD who were followed at the PCD center in Puerto Rico and were homozygous for c.921+3_921+6delAAGT genetic variant. Demographic data (age at evaluation and sex), spirometry (FEV_1 as percentage predicted using Global Lung Index (GLI) 2012 reference equations), and chest CT imaging (Digital Imaging and Communications in Medicine files—DICOM) were extracted from the medical record. Clinical and imaging data were obtained from medical records spanning (2021–2026). Because specialized PCD diagnostic services in Puerto Rico were established relatively recently, several participants were diagnosed later in life; therefore, age at diagnosis should not be interpreted as reflecting the age of disease onset. For participants with more than one available chest CT, the most recent CT examination was selected for analysis. Spirometry was obtained from the pulmonary function assessment performed closest in time to the selected CT examination. This approach provided one cross-sectional imaging and pulmonary function data set per participant and was used consistently across the cohort.

2.2. Imaging Scoring

A composite Bhalla-style score was used as the per-patient imaging severity metric [10]. The lungs were divided into six anatomical regions: the right upper, middle, and lower lobes; the left upper and lower lobes; and the lingula. Each region was evaluated separately for five CT abnormalities by a single scorer: bronchiectasis, mucous plugging, peribronchial thickening, parenchymal abnormalities, and pulmonary hyperinflation. Mucous plugging, peribronchial thickening, parenchymal abnormalities, and hyperinflation were scored as either absent (0 points) or present (1 point). Bronchiectasis was graded according to the diameter of the bronchus relative to the adjacent pulmonary artery: absent (0 points), mild at 1–2 times the arterial diameter (1 point), moderate at 2–3 times the arterial diameter (2 points), or severe at greater than 3 times the arterial diameter (3 points). Therefore, each region could receive a maximum score of 7 points, 3 points for bronchiectasis and 1 point for each of the other four features, resulting in a total lung score ranging from 0, indicating a normal CT examination, to 42, indicating severe disease across all six regions. In this

scoring system, higher scores indicate greater structural lung disease burden; a score of 0 represents no scored CT abnormalities, whereas a score of 42 represents the maximum measurable disease burden.

2.3. Statistical Analysis

Continuous variables are reported as mean ± SD and median (IQR), and categorical variables as *n* (%). Pearson and Spearman correlations were calculated for relationships among age, FEV_1, and CT severity. Univariable linear regression was used to estimate the slopes of FEV_1 and CT score with age. A multivariable ordinary-least-squares model regressed FEV_1 on age, sex, and CT score. Tests were two-sided with $\alpha = 0.05$. Analyses were performed in Python 3 using NumPy and pandas; Pearson, Spearman, and ordinary least squares (OLS) statistics were implemented from first principles to reproduce standard reference statistics.

3. Results

3.1. Demographics, Lung Function, and CT Severity

The cohort comprised 20 founder-variant homozygotes (12 female, 60%) ranging from 5 to 63 years of age (mean 33.4 ± 19.4 years). Mean FEV_1 was 48.9 ± 10.2% predicted (range 26–65%), and the mean Bhalla-style CT score was 13.8 ± 8.2. Detailed demographic, lung-function, pseudomonas aeruginosa and imaging characteristics are summarized in Table 1.

Table 1. Demographics, lung function, and CT severity of the *RSPH4A* founder-homozygous cohort.

Variable	Founder-Homozygous Cohort (*n* = 20)
Female, *n* (%)	12 (60%)
Male, *n* (%)	8 (40%)
Age, mean ± SD (yr)	33.4 ± 19.4
Age, median (IQR)	24 (20–51)
Age range (yr)	5–63
FEV_1, mean ± SD (% pred)	48.9 ± 10.2
FEV_1, median (IQR)	48 (42–58)
FEV_1 range (%)	26–65
Pseudomonas aeruginosa colonization	20 (100%)
CT score, mean ± SD	13.8 ± 8.2
CT score, median (IQR)	13 (8–18)

FEV_1, forced expiratory volume in 1 s; CT, computed tomography; IQR, interquartile range. CT score uses a Bhalla-style lobar grading system.

3.2. CT Imaging in RSPH4A, c.921+3_921+6delAAGT Founder Variant

Chest CT demonstrated a broad spectrum of structural lung abnormalities among patients homozygous for the *RSPH4A* c.921+3_921+6delAAGT founder variant. Across age groups, abnormalities included airway dilation, bronchial wall thickening, mucus plugging, air trapping, tree-in-bud opacities, bronchiolitis, ground-glass opacities, architectural distortion, segmental collapse, and bronchiectasis. Representative axial and coronal images illustrate increasing structural complexity across the age spectrum, with more extensive bronchiectasis and parenchymal abnormalities apparent in older patients (Figure 1). This qualitative pattern complements the quantitative CT scoring used throughout the cohort.

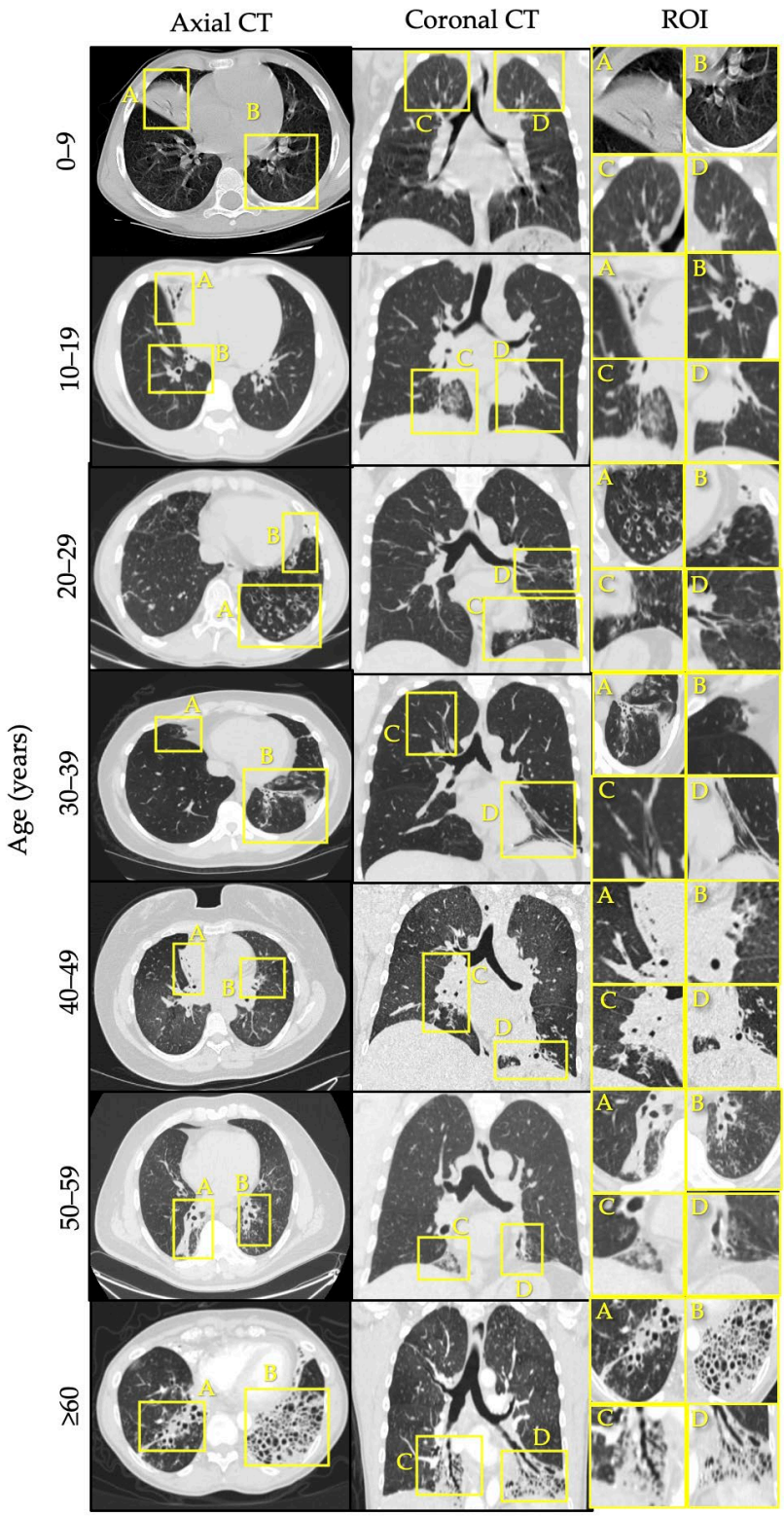


Figure 1. Age-related progression of structural lung abnormalities on chest CT. Representative axial and coronal CT images are shown across age groups from 0–9 years to ≥60 years. Yellow boxes labeled A–D identify selected regions of interest (ROIs), with corresponding magnified views displayed in the right column. The images demonstrate progressive structural lung abnormalities with increasing age, including airway dilation, bronchial wall thickening, mucus plugging, parenchymal opacities, and increasingly extensive bronchiectasis changes, most pronounced in the older age groups.

High-resolution CT further demonstrated the heterogeneity of the pulmonary phenotype, ranging from small-airway and parenchymal abnormalities to established bronchiectasis remodeling (Figure 2).

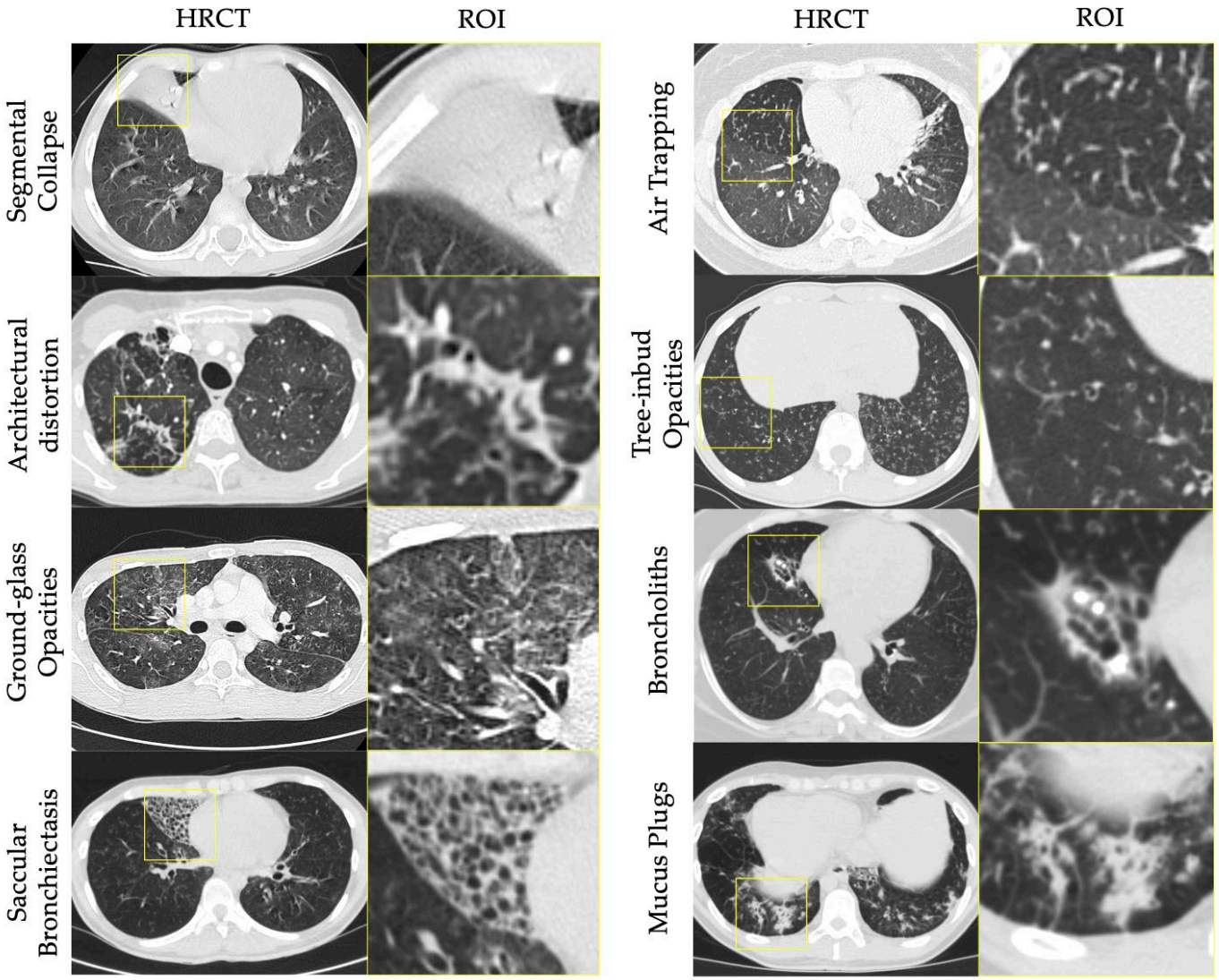


Figure 2. Representative computed tomography (CT) findings in patients with primary ciliary dyskinesia (PCD) due to the Puerto Rican *RSPH4A* founder variant. Representative axial CT images from patients with the *RSPH4A* c.921+3_921+6delAAGT founder variant demonstrate the spectrum of structural pulmonary abnormalities observed in the cohort, including segmental collapse, architectural distortion, ground-glass opacities, saccular bronchiectasis, air trapping, tree-in-bud opacities, broncholiths, and mucus plugging. Yellow boxes identify regions of interest (ROIs), with corresponding magnified views displayed adjacent to each CT image to highlight the characteristic abnormalities. Collectively, these findings illustrate the heterogeneous airway and parenchymal involvement associated with *RSPH4A*-related PCD.

Bronchiectasis exhibited variable morphology, including cylindrical, varicose, and cystic patterns. Representative coronal images illustrate this morphological spectrum from relatively preserved airway caliber to progressively irregular airway dilatation and cystic remodeling (Figure 3). Collectively, these findings demonstrate substantial structural lung involvement in *RSPH4A*-related PCD and provide the imaging context for the subsequent quantitative analyses of CT severity, age, and pulmonary function.

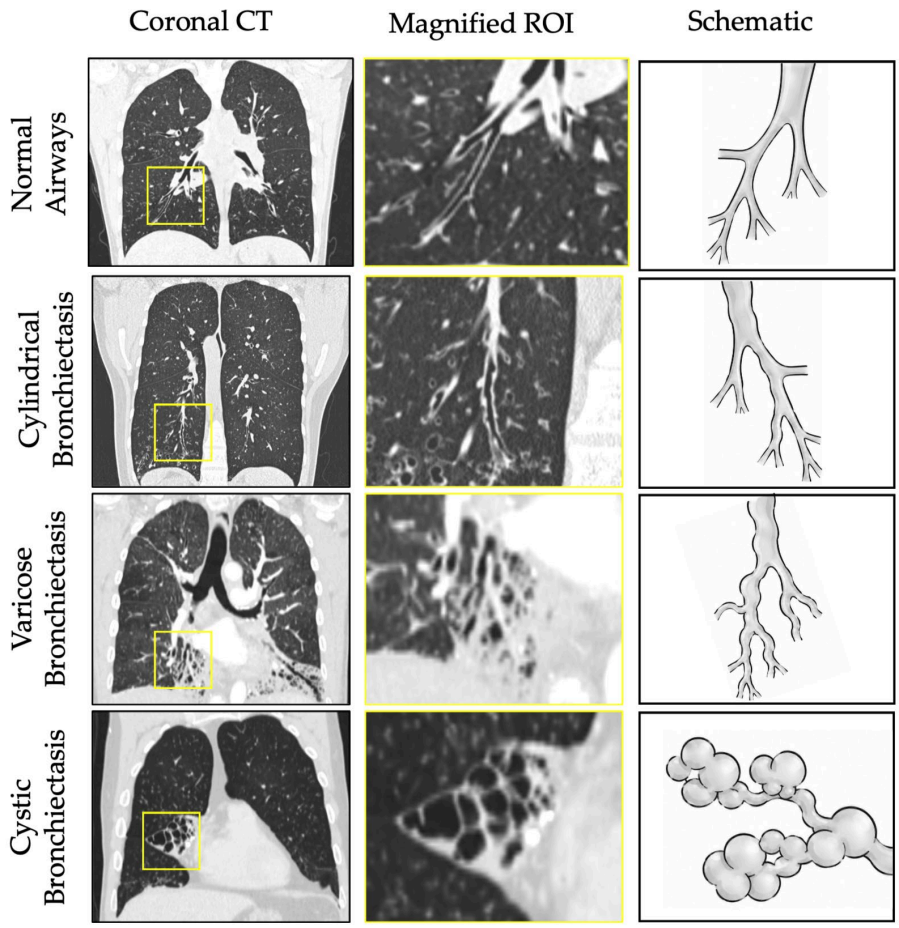


Figure 3. Morphologic spectrum of bronchiectasis in *RSPH4A*-related primary ciliary dyskinesia. Representative coronal computed tomography (CT) images from patients with primary ciliary dyskinesia (PCD) harboring the Puerto Rican *RSPH4A* c.921+3_921+6delAAGT founder variant illustrate progressive morphologic patterns of airway dilatation. Images demonstrate normal airways, cylindrical bronchiectasis characterized by relatively uniform bronchial dilatation, varicose bronchiectasis characterized by irregular bronchial caliber with alternating areas of dilatation and narrowing, and cystic bronchiectasis characterized by markedly dilated, sac-like distal airways. Yellow boxes indicate regions of interest (ROIs), which are shown at higher magnification in the center column. Corresponding schematics in the right column illustrate the characteristic airway morphology of each pattern.

3.3. Age-Related Trajectory of Lung Function and CT Severity

FEV_1 showed no measurable decline with age in the founder cohort: linear-regression slope = −0.02% per year (95% CI −0.26 to +0.22; R^2 = 0.001; p = 0.88). The Pearson correlation between age and FEV_1 was −0.04 (95% CI −0.47 to +0.41; p = 0.88), and the Spearman ρ was −0.03 (p = 0.91). The flat trajectory is consistent with an early-established, fixed obstructive deficit rather than progressive decline (Figure 4A). CT severity, in contrast, drifted upward with age (Pearson r = +0.33, 95% CI −0.13 to +0.68; p = 0.15), although this association was not statistically significant, and total bronchiectasis severity correlated more strongly (Pearson r = +0.43, 95% CI −0.02 to +0.73; p = 0.06), which approached but did not reach statistical significance. Linear regression of CT score on age gave a slope of +0.14 points per year (R^2 = 0.11), translating to roughly +1.4 points per decade (Figure 4B). The apparent age-related increase in CT severity was influenced by one older adult with a particularly high CT severity score, while the remaining adult participants generally had lower scores. Thus, the cross-sectional trend should not be interpreted as evidence of uniform progressive structural disease across all individuals. Imaging severity

inversely correlated with FEV_1 in the founder cohort (Pearson r = −0.40, 95% CI −0.71 to +0.06; $p = 0.08$; Spearman ρ = −0.37, $p = 0.11$). Univariable linear regression yielded a slope of −0.49% FEV_1 per CT point ($R^2 = 0.16$; $p = 0.08$; Figure 4C)—imaging burden, not chronological age, captured most of the functional variability. Within the founder cohort, females ($n = 12$) had numerically higher CT scores (14.7 ± 8.7 vs. 12.4 ± 7.9) and slightly higher FEV_1 (50.2 ± 9.3% vs. 47.0 ± 11.7%) than males ($n = 8$), with no statistically significant differences (all $p > 0.25$) (Figure 4D).

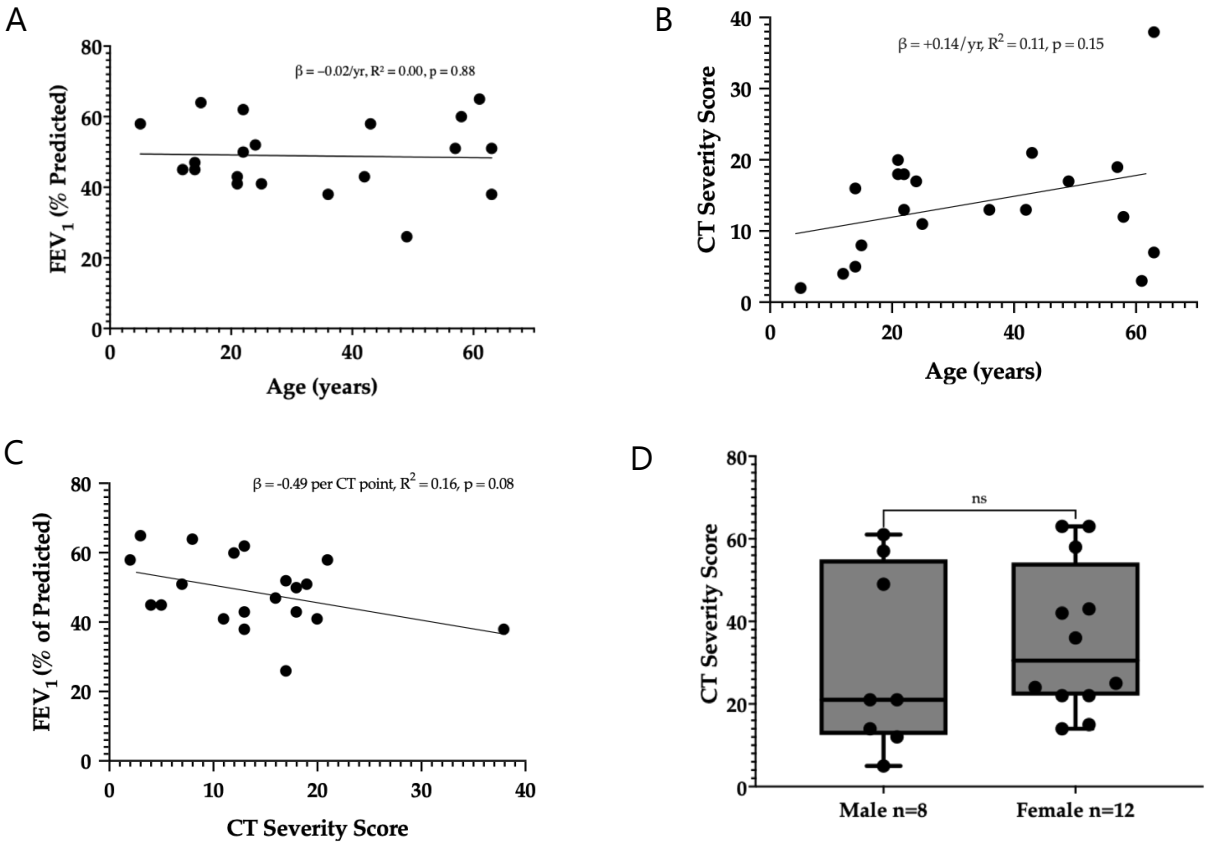


Figure 4. Associations between age, lung function, and structural lung disease in the *RSPH4A* founder-homozygous cohort (n = 20). (**A**) FEV_1 remained stable across age, with values consistently below the lower limit of normal (80%, dotted line). (**B**) CT severity showed a modest increase with age. (**C**) Greater CT disease burden was associated with lower FEV_1. (**D**) CT severity scores were compared between male and female participants. Females had numerically higher CT severity scores than males, although the difference was not statistically significant ($p > 0.05$). Solid lines in panels A–C represent linear regression fits. FEV_1, forced expiratory volume in 1 s; CT, computed tomography; ns, not significant.

3.4. Lobar Bronchiectasis Distribution

Bronchiectasis was multilobar with right-middle-lobe (RML) predominance: 80% of founder homozygotes had RML involvement, followed by the left lower lobe (75%), right lower lobe (60%), and lingula (55%) (Table 2). An OLS model regressing FEV_1 on age, sex, and CT score in the founder cohort identified CT score as the only predictor approaching significance (β = −0.56% per CT point, 95% CI −1.13 to +0.01; $p = 0.07$). Age and sex contributed negligibly once imaging severity was included. The model explained 21% of FEV_1 variance ($R^2 = 0.21$; $n = 20$) (Table 3). Stratifying the founder cohort by age showed reduced mean FEV_1 among participants <18 years ($n = 5$: mean 51.8% predicted; CT score 7.0), with higher mean CT severity in young adulthood (18–39 years, $n = 7$: FEV_1 46.7%; CT score 15.7) and adulthood (≥40 years, $n = 8$: FEV_1 49.0%; CT score

16.2). Importantly, the 0–9-year age group included only one participant with available spirometry; therefore, this individual's FEV_1 should not be considered representative of lung function in young children with this founder variant. Mean CT severity more than doubled between childhood and adulthood while FEV_1 stayed near 50% predicted, consistent with the fixed-deficit/accruing-structure pattern.

Table 2. Lobar bronchiectasis prevalence in the founder-homozygous cohort.

Lobe	Founder Cohort, *n* (%)
Right upper (RUL)	6 (30%)
Right middle (RML)	16 (80%)
Right lower (RLL)	12 (60%)
Left upper (LUL)	2 (10%)
Lingula	11 (55%)
Left lower (LLL)	15 (75%)

Table 3. Multivariable OLS regression—FEV_1 on age, sex, and CT score (founder-homozygous cohort, $n = 20$).

Predictor	β (95% CI)	Standard Error	*p*-Value
Intercept	56.8 (45.4 to 68.2)	5.81	<0.001
Age (per year)	+0.04 (−0.20 to +0.29)	0.12	0.73
Male sex	−4.20 (−13.14 to +4.73)	4.56	0.37
CT score (per point)	−0.56 (−1.13 to +0.01)	0.29	0.07

4. Discussion

This study provides, to our knowledge, the first dedicated genotype–computed tomography (CT) phenotype characterization of patients homozygous for the Puerto Rican *RSPH4A* founder variant, c.921+3_921+6delAAGT, building on earlier descriptions of the clinical presentation and population genetics of this founder allele [8,9]. Three principal observations emerged from this 20-patient cohort. First, airflow obstruction was substantial and remarkably uniform, with a mean FEV_1 of 48.9% predicted across the full age range studied. Second, structural CT burden increased progressively with age even though FEV_1 remained essentially unchanged over the same interval, more than doubling in mean CT score between childhood and adulthood. Third, bronchiectasis was consistently multilobar, with a right-middle-lobe predominance (80%) accompanied by frequent left lower lobe, right lower lobe, and lingular involvement. Taken together, these observations begin to define a distinct structural and functional pulmonary phenotype for *RSPH4A*-related PCD in the Puerto Rican founder population and indicate that functional and structural disease evolve along divergent trajectories in this genotype.

The most striking functional finding was the absence of any measurable decline in FEV_1 with age (slope −0.02% per year; 95% CI −0.26 to +0.22; $p = 0.88$). Rather than reflecting genuine disease stability, this flat cross-sectional trajectory is better explained by an obstructive deficit that is established early in life and subsequently preserved at a relatively fixed level: FEV_1 was already reduced to a mean of 51.8% predicted in patients younger than 18 years and remained close to 50% predicted in both the young-adult and adult strata. This pattern contrasts with the more heterogeneous, and on average modestly declining, longitudinal trajectories reported in larger, genetically mixed PCD cohorts, where mean annual FEV_1 has been estimated to fall by roughly 0.06–0.11 z-scores per year with substantial inter-individual variability [11,12]. It is also consistent with observations that lung function in PCD can deteriorate before diagnosis and then stabilize once patients are established in specialized care [13]. We therefore interpret the flat FEV_1–age relationship in this founder cohort as evidence of an early-established functional ceiling effect rather than proof that the underlying disease process is quiescent.

In contrast to the flat spirometry trajectory, structural disease appeared to progress steadily with age. CT severity increased by an estimated 1.4 points per decade ($R^2 = 0.11$) and total bronchiectasis severity correlated even more strongly with age (Pearson r = +0.43; $p = 0.06$), while mean FEV_1 changed by only a fraction of a percentage point across the same age strata. This dissociation between preserved spirometry and accumulating structural abnormality mirrors observations in cystic fibrosis, where CT scores have been shown to worsen significantly over time even when FEV_1 remains stable or improves [14], and parallels reports in PCD cohorts in which CT severity, exacerbation frequency, and chronic infection correspond more closely with structural change more closely than with spirometry decline [15,16]. Because FEV_1 is a global, effort-dependent measure that reflects the combined mechanical output of all lung units, focal or multilobar structural injury, of the kind demonstrated here, can accumulate substantially before it is reflected in a measurable fall in FEV_1. These findings suggest that spirometry alone may underestimate the true burden and trajectory of structural lung disease in *RSPH4A*-related PCD.

The CT phenotype observed across the cohort was broad and heterogeneous, encompassing airway dilation, bronchial wall thickening, mucus plugging, air trapping, tree-in-bud opacities, bronchiolitis, ground-glass opacities, architectural distortion, segmental collapse, and bronchiectasis. This constellation is consistent with previously described high-resolution CT features of PCD, which similarly emphasize mucous plugging, tree-in-bud pattern, and atelectasis as characteristic findings [17,18]. Bronchiectasis itself spanned the full morphologic spectrum, from cylindrical to varicose to cystic disease, sometimes within the same patient. This heterogeneity likely reflects variable regional exposure to recurrent infection and inflammation over time in the setting of impaired mucociliary clearance, producing airway remodeling that ranges from early, potentially more reversible dilation to fixed, saccular destruction [19]. The coexistence of small-airway findings (air trapping, tree-in-bud opacities, bronchiolitis) alongside established bronchiectasis in the same cohort suggests that the founder-variant phenotype includes both active small-airway disease and its downstream structural sequelae.

Bronchiectasis distribution was multilobar but not uniform: right-middle-lobe involvement was present in 80% of patients, followed by the left lower lobe (75%), right lower lobe (60%), and lingula (55%), with comparatively less upper-lobe disease. A middle- and lower-lobe-predominant, right-middle-lobe/lingula-weighted pattern has previously been reported as a typical, though not PCD-specific, feature of PCD-related bronchiectasis more broadly [17,18], and has even been incorporated as a discriminating feature in diagnostic scoring systems for bronchiectasis of unclear etiology. The consistency of this pattern within our genetically homogeneous cohort raises the possibility that it represents a recognizable imaging signature of the Puerto Rican *RSPH4A* founder genotype specifically, potentially related to regional differences in airway geometry, gravitational dependency, or baseline mucus clearance efficiency. However, because this study lacked a comparator cohort of patients with other PCD-causing genotypes or non-PCD bronchiectasis, we cannot distinguish a genotype-specific distribution from a distribution that is characteristic of PCD in general. Confirming whether this lobar pattern is unique to *RSPH4A*-related disease will require direct comparison with other PCD genotypes.

CT severity was the variable most closely linked to FEV_1 in this cohort. Imaging burden correlated inversely with FEV_1 (Pearson r = −0.40; $p = 0.08$), and in the multivariable model that included age, sex, and CT score, CT score was the only variable that approached statistical significance ($\beta = -0.56\%$ FEV_1 per CT point; 95% CI −1.13 to +0.01; $p = 0.07$), while age and sex contributed little once imaging severity was accounted for, and the model explained only a modest proportion of FEV_1 variance ($R^2 = 0.21$). This pattern is broadly consistent with prior work linking automated and visual CT scores

to spirometry impairment in PCD [15,16]. Given the small sample size inherent to this genetically homogeneous founder cohort, the study has limited precision for detecting modest associations, as reflected by confidence intervals that include the null and *p*-values above the conventional threshold for statistical significance. Accordingly, the observed relationships should be interpreted primarily in terms of their estimated magnitude, direction, and uncertainty rather than as definitive evidence of association. Nevertheless, several analyses demonstrated directionally consistent patterns. Greater CT disease burden was associated with lower FEV_1 in both univariable analysis ($\beta = -0.49\%$ FEV_1 per CT point; $p = 0.08$) and the multivariable model adjusted for age and sex ($\beta = -0.56\%$ per CT point; 95% CI, −1.13 to +0.01; $p = 0.07$). Similarly, CT severity and bronchiectasis burden tended to increase with age, whereas FEV_1 showed essentially no cross-sectional relationship with age. These concordant trends are clinically informative and generate hypotheses regarding a possible dissociation between structural and functional disease burden; however, they do not constitute definitive statistical evidence of these associations. The uncertainty arises principally from the limited number of individuals available with this rare founder genotype and the resulting wide confidence intervals. Confirmation will require longitudinal follow-up of this cohort and, where feasible, larger collaborative studies of patients carrying the same variant.

These findings are plausible considering the predicted molecular consequences of c.921+3_921+6delAAGT. This 4-nucleotide deletion disrupts the canonical splice donor site of *RSPH4A* intron 6 and is predicted to cause exon 6 skipping or intron retention, generating a frameshifted transcript that is targeted for degradation by nonsense-mediated decay; functionally, it is expected to behave as a near-null, loss-of-function allele, an interpretation supported by prior characterization of this founder variant and its ancestral origin in the Puerto Rican population [7,8]. *RSPH4A* is a core structural component of the radial spoke head, which physically couples the axonemal central-pair apparatus to the dynein regulatory machinery and is required for normal, coordinated ciliary beating [4]. Near-complete loss of *RSPH4A* function would therefore be expected to produce severe, early, and relatively uniform impairment of ciliary beat and mucociliary clearance from birth, consistent with our biophysical characterization of ciliary beat abnormalities in this same founder variant [20]. We speculate that this severe, early ciliary dysfunction could drive early airway injury, manifesting as the fixed obstructive deficit already present in childhood, while impaired clearance of secretions and recurrent infection and inflammation continue to remodel the airways over subsequent decades, producing the progressive structural findings observed on CT [19]. This two-phase interpretation, an early, largely fixed functional insult followed by a slower, cumulative structural process, is offered as a plausible biological framework rather than a mechanism directly demonstrated by this cross-sectional dataset.

These findings carry several clinical implications. First, because FEV_1 appeared to plateau early and did not correspond with the ongoing accumulation of structural disease, FEV_1 alone may not adequately capture the true evolution of lung disease in *RSPH4A*-related PCD, and structural imaging surveillance may provide complementary prognostic information not captured by spirometry [14,15]. Second, given that substantial functional impairment already appears to be established during childhood, early diagnosis is likely to be particularly important in this population, since interventions initiated after a fixed deficit has developed may have a narrower window in which to alter the disease trajectory; earlier recognition and diagnosis have been associated with more favorable outcomes in other PCD cohorts [13]. Third, recognition of the distinctive clinical and radiographic phenotype associated with this founder variant, together with the availability of confirmatory genetic testing [20], may support population-specific diagnostic pathways, including a lower

threshold for genetic testing among Puerto Rican patients with unexplained bronchiectasis or an RML-predominant pattern, and could inform the feasibility of targeted screening strategies in this population [8,9].

This study has several notable strengths, including a genetically homogeneous cohort restricted to confirmed homozygotes for a single founder variant, detailed Bhalla-style CT phenotyping across six anatomical regions, systematic lobar assessment of bronchiectasis, and integration of imaging findings with spirometry data. These strengths are balanced by important limitations. The sample size was small (n = 20), which limited statistical power and likely explains why several associations, including the CT–FEV_1 relationship, approached but did not reach conventional significance. The cohort was drawn from a single center, single scorer, and a single founder population, which may limit generalizability. The design was cross-sectional rather than longitudinal, and no comparator cohort of patients with other PCD-causing genotypes or with non-PCD bronchiectasis was available, limiting our ability to determine whether the observed imaging phenotype and lobar distribution are specific to this genotype. Differences in treatment intensity, disease duration, and unmeasured comorbidities could also have confounded the observed age-related patterns. The heterogeneity of CT findings despite a shared homozygous founder genotype also suggests that non-genetic modifiers, including environmental exposures, infection history, treatment intensity, and other clinical factors, may contribute substantially to the structural pulmonary phenotype and should be systematically evaluated in future longitudinal studies. Most importantly, because these data are cross-sectional, the apparent age-related increase in CT severity reflects a comparison across different individuals at different ages rather than documented progression within the same patients over time, and it therefore cannot establish individual longitudinal trajectories of structural disease.

Future work should prioritize longitudinal follow-up with paired CT and pulmonary-function testing in the same individuals to directly test whether structural disease progresses within patients as it appears to across the cohort cross-sectionally. Larger, multicenter cohorts, potentially through collaboration with PCD registries in other centers, will be needed to confirm these associations with adequate statistical power and to determine whether the imaging phenotype and lobar distribution described here are specific to the *RSPH4A* founder genotype or shared across other PCD-causing variants [11,12]. Quantitative and automated CT analysis methods may offer more reproducible and sensitive measures of structural change than visual scoring alone [15], and complementary physiologic biomarkers, such as lung clearance index or other measures of ventilation heterogeneity, could help detect early functional decline that FEV_1 fails to capture. In summary, the Puerto Rican *RSPH4A* founder phenotype appears to be characterized by an early-established obstructive deficit accompanied by continued accumulation of structural lung injury, a pattern in which imaging serves as an essential complement to spirometry for understanding the true burden of disease in this population.

5. Conclusions

This study defines a structural and functional lung phenotype associated with homozygosity for the Puerto Rican *RSPH4A* c.921+3_921+6delAAGT founder variant. Affected individuals demonstrated substantial airflow obstruction that was already evident in childhood and remained relatively stable across age, while CT abnormalities accumulated with increasing age and encompassed progressive bronchiectasis, mucus plugging, small-airway disease, and parenchymal remodeling. Bronchiectasis was characteristically multilobar, with prominent right-middle-lobe involvement, and greater CT disease burden was associated with lower FEV_1. Together, these findings suggest that spirometry alone may incompletely reflect the evolution of structural lung disease in this genotype

and support the complementary role of CT imaging in longitudinal assessment. Recognition of this genotype-specific phenotype may facilitate earlier identification, improve disease monitoring, and inform future natural-history studies and targeted interventions for *RSPH4A*-related PCD.

Author Contributions: Conceptualization, W.D.J.-R., J.E.P.M. and R.A.M.; methodology, W.D.J.-R., J.E.P.M., M.J.R.-B. and G.R.-O.; formal analysis, W.D.J.-R., J.E.P.M. and G.R.-O.; investigation, J.E.P.M., G.R.-O. and W.D.J.-R.; data curation, J.E.P.M. and G.R.-O.; visualization, J.E.P.M., G.R.-O., M.J.R.-B. and W.D.J.-R.; writing—original draft preparation, J.E.P.M. and W.D.J.-R.; writing—review and editing, G.R.-O., M.J.R.-B., R.A.M. and W.D.J.-R.; supervision, W.D.J.-R. and R.A.M.; project administration, W.D.J.-R.; funding acquisition, R.A.M. and W.D.J.-R. All authors have read and agreed to the published version of the manuscript.

Funding: This work was supported by the Puerto Rico PCD Foundation, the Research Centers in Minority Institutions (RCMI) Center for Research Resources, and the Molecular and Genomics Core (Grant No. U54MD007579). The authors sincerely thank the Graham family for their generous support, which made this study possible.

Institutional Review Board Statement: The study was conducted in accordance with the Declaration of Helsinki and approved by the Institutional Review Board of Ponce Health Sciences University (protocol code 2512299384, date of approval: 7 January 2026).

Informed Consent Statement: Informed consent was obtained from all subjects involved in the study.

Data Availability Statement: The raw data supporting the conclusions of this article will be made available by the authors on request.

Conflicts of Interest: The authors declare no conflict of interest.

Abbreviations

The following abbreviations are used in this manuscript:

CI	Confidence interval
CT	Computed tomography
DICOM	Digital Imaging and Communications in Medicine
FEV_1	Forced expiratory volume in 1 s
GLI	Global Lung Function Initiative
IQR	Interquartile range
LLL	Left lower lobe
LUL	Left upper lobe
OLS	Ordinary least squares
PCD	Primary ciliary dyskinesia
RLL	Right lower lobe
RML	Right middle lobe
ROI	Region of interest
RSPH4A	Radial spoke head component 4A
RUL	Right upper lobe
SD	Standard deviation

References

1. Despotes, K.A.; Zariwala, M.A.; Davis, S.D.; Ferkol, T.W. Primary Ciliary Dyskinesia: A Clinical Review. *Cells* **2024**, *13*, 974. [CrossRef]
2. Hannah, W.B.; Seifert, B.A.; Truty, R.; Zariwala, M.A.; Ameel, K.; Zhao, Y.; Nykamp, K.; Gaston, B. The Global Prevalence and Ethnic Heterogeneity of Primary Ciliary Dyskinesia Gene Variants: A Genetic Database Analysis. *Lancet Respir. Med.* **2022**, *10*, 459–468. [CrossRef]

3. Castleman, V.H.; Romio, L.; Chodhari, R.; Hirst, R.A.; de Castro, S.C.; Parker, K.A.; Ybot-Gonzalez, P.; Emes, R.D.; Wilson, S.W.; Wallis, C.; et al. Mutations in Radial Spoke Head Protein Genes *RSPH9* and *RSPH4A* Cause Primary Ciliary Dyskinesia with Central-Microtubular-Pair Abnormalities. *Am. J. Hum. Genet.* **2009**, *84*, 197–209. [CrossRef]
4. Zhao, Y.; Pinskey, J.M.; Lin, J.; Yin, W.; Sears, P.R.; Daniels, L.A.; Zariwala, M.A.; Knowles, M.R.; Ostrowski, L.E.; Nicastro, D. Structural Insights into the Cause of Human *RSPH4A* Primary Ciliary Dyskinesia. *Mol. Biol. Cell* **2021**, *32*, 1202–1209. [CrossRef]
5. Shoemark, A.; Goutaki, M.; Kinghorn, B.; Ardura-Garcia, C.; Baz-Redón, N.; Chilvers, M.; Davis, S.D.; De Brandt, J.; Dell, S.; Dhar, R.; et al. European Respiratory Society and American Thoracic Society Guidelines for the Diagnosis of Primary Ciliary Dyskinesia. *Eur. Respir. J.* **2025**, *66*, 2500745. [CrossRef]
6. Leigh, M.W.; Hazucha, M.J.; Chawla, K.K.; Baker, B.R.; Shapiro, A.J.; Brown, D.E.; LaVange, L.M.; Horton, B.J.; Qaqish, B.; Carson, J.L.; et al. Standardizing Nasal Nitric Oxide Measurement as a Test for Primary Ciliary Dyskinesia. *Ann. Am. Thorac. Soc.* **2013**, *10*, 574–581. [CrossRef]
7. Daniels, M.L.; Leigh, M.W.; Davis, S.D.; Armstrong, M.C.; Carson, J.L.; Hazucha, M.; Dell, S.D.; Eriksson, M.; Collins, F.S.; Knowles, M.R.; et al. Founder Mutation in *RSPH4A* Identified in Patients of Hispanic Descent with Primary Ciliary Dyskinesia. *Hum. Mutat.* **2013**, *34*, 1352–1356. [CrossRef]
8. De Jesús-Rojas, W.; Reyes De Jesús, D.; Nieves, A.M.; Mosquera, R.A.; Martínez-Cruzado, J.C. Primary Ciliary Dyskinesia: Ancestral Haplotypes Analysis of the *RSPH4A* Founder Mutation in Puerto Rico. *Cureus* **2021**, *13*, e17673. [CrossRef]
9. De Jesús-Rojas, W.; Reyes-De Jesús, D.; Mosquera, R.A. Primary Ciliary Dyskinesia Diagnostic Challenges: Understanding the Clinical Phenotype of the Puerto Rican *RSPH4A* Founder Mutation. *Diagnostics* **2021**, *11*, 281. [CrossRef]
10. Bhalla, M.; Turcios, N.; Aponte, V.; Jenkins, M.; Leitman, B.S.; McCauley, D.I.; Naidich, D.P. Cystic Fibrosis: Scoring System with Thin-Section CT. *Radiology* **1991**, *179*, 783–788. [CrossRef]
11. Halbeisen, F.S.; Pedersen, E.S.L.; Goutaki, M.; Spycher, B.D.; Amirav, I.; Boon, M.; Cohen-Cymberknoh, M.; Gartner, S.; Kobbernagel, H.E.; Kouis, P.; et al. Lung Function from School Age to Adulthood in Primary Ciliary Dyskinesia. *Eur. Respir. J.* **2022**, *60*, 2101918. [CrossRef]
12. Gatt, D.; Shaw, M.; Kritzinger, F.; Solomon, M.; Dell, S.; Ratjen, F. The Impact of Age of Diagnosis in Children with Primary Ciliary Dyskinesia. *Ann. Am. Thorac. Soc.* **2025**, *22*, 208–215. [CrossRef]
13. de Jong, P.A.; Nakano, Y.; Lequin, M.H.; Mayo, J.R.; Woods, R.; Paré, P.D.; Tiddens, H.A.W.M. Progressive Damage on High Resolution Computed Tomography Despite Stable Lung Function in Cystic Fibrosis. *Eur. Respir. J.* **2004**, *23*, 93–97. [CrossRef]
14. Hoang-Thi, T.N.; Revel, M.P.; Burgel, P.R.; Bassinet, L.; Honoré, I.; Hua-Huy, T.; Martin, C.; Maitre, B.; Chassagnon, G. Automated Computed Tomographic Scoring of Lung Disease in Adults with Primary Ciliary Dyskinesia. *BMC Pulm. Med.* **2018**, *18*, 194. [CrossRef]
15. Piatti, G.; De Santi, M.M.; Farolfi, A.; Zuccotti, G.V.; D'Auria, E.; Patria, M.F.; Torretta, S.; Consonni, D.; Ambrosetti, U. Exacerbations and Pseudomonas Aeruginosa Colonization Are Associated with Altered Lung Structure and Function in Primary Ciliary Dyskinesia. *BMC Pediatr.* **2020**, *20*, 158. [CrossRef]
16. Kennedy, M.P.; Noone, P.G.; Leigh, M.W.; Zariwala, M.A.; Minnix, S.L.; Knowles, M.R.; Molina, P.L. High-Resolution CT of Patients with Primary Ciliary Dyskinesia. *AJR Am. J. Roentgenol.* **2007**, *188*, 1232–1238. [CrossRef]
17. Dettmer, S.; Ringshausen, F.C.; Vogel-Claussen, J.; Fuge, J.; Faschkami, A.; Shin, H.O.; Schwerk, N.; Welte, T.; Wacker, F.; Rademacher, J. Computed Tomography in Adult Patients with Primary Ciliary Dyskinesia: Typical Imaging Findings. *PLoS ONE* **2018**, *13*, e0191457. [CrossRef]
18. Flume, P.A.; Chalmers, J.D.; Olivier, K.N. Advances in Bronchiectasis: Endotyping, Genetics, Microbiome, and Disease Heterogeneity. *Lancet* **2018**, *392*, 880–890. [CrossRef]
19. Rosario-Ortiz, G.; Muñiz-Hernández, J.; Ortiz-Pérez, N.M.; Ramos-Benitez, M.J.; Mosquera, R.A.; De Jesús-Rojas, W. Cilia Dynamics in Primary Ciliary Dyskinesia: A Biophysical Characterization of the *RSPH4A* Founder Variant. *Cells* **2026**, *15*, 607. [CrossRef]
20. Collins, S.A.; Walker, W.T.; Lucas, J.S. Genetic Testing in the Diagnosis of Primary Ciliary Dyskinesia: State-of-the-Art and Future Perspectives. *J. Clin. Med.* **2014**, *3*, 491–503. [CrossRef]

Disclaimer/Publisher's Note: The statements, opinions and data contained in all publications are solely those of the individual author(s) and contributor(s) and not of MDPI and/or the editor(s). MDPI and/or the editor(s) disclaim responsibility for any injury to people or property resulting from any ideas, methods, instructions or products referred to in the content.